Crossover from Linear to Quadratic Electro-optic Behavior in BaTiO3 and (Ba, Sr)TiO3 Solid Solution

Sergey Prosandeev, Charles Paillard, L. Bellaiche

▶ **To cite this version:**

Sergey Prosandeev, Charles Paillard, L. Bellaiche. Crossover from Linear to Quadratic Electro-optic Behavior in BaTiO3 and (Ba, Sr)TiO3 Solid Solution. Physical Review Letters, 2024, 132 (19), pp.196901. 10.1103/PhysRevLett.132.196901 . hal-04571468

HAL Id: hal-04571468

https://centralesupelec.hal.science/hal-04571468

Submitted on 7 May 2024

HAL is a multi-disciplinary open access archive for the deposit and dissemination of scientific research documents, whether they are published or not. The documents may come from teaching and research institutions in France or abroad, or from public or private research centers.

L'archive ouverte pluridisciplinaire **HAL**, est destinée au dépôt et à la diffusion de documents scientifiques de niveau recherche, publiés ou non, émanant des établissements d'enseignement et de recherche français ou étrangers, des laboratoires publics ou privés.

Crossover from linear to quadratic electro-optic behavior in $BaTiO_3$ and (Ba,Sr)TiO_3 solid solution

Sergey Prosandeev,[1,*] Charles Paillard,[1,2,†] and L. Bellaiche[1,‡]

[1] *Institute of Nanoscience Physics and Physics Department, University of Arkansas, Fayetteville, Arkansas 72701, USA*

[2] *Université Paris-Saclay, CentraleSupélec, CNRS, Laboratoire SPMS, 91190, Gif-sur-Yvette, France.*

(Dated:)

Abstract

We derive a numerical method based on coupled Density Functional Theory and effective Hamiltonian schemes to calculate the linear and quadratic electro-optic response of ferroelectrics at finite temperature and in different frequency ranges. By applying the developed method to $BaTiO_3$, we successfully resolve apparent discrepancies in the experimental literature which reported a linear or quadratic electro-optic response when visible or THz radiation was employed to measure the optical index, respectively. We further demonstrate that (and explain why), in the case of the (Ba,Sr)TiO_3 disordered solid solutions, structural phase transitions not only lead to larger linear electro-optic constants, as previously demonstrated in the literature, but also significantly enhance the quadratic electro-optic constants.

Ferroelectric materials, such as $BaTiO_3$ (BTO) or $LiNbO_3$, attract particular attention for optical applications. Their strong electro-optic (EO) response, that is the significant change of the refractive indices under an applied low-frequency electric field, is key to EO modulators, sensors, scramblers, compensation modules, or holographic storage technologies [1].

Original and subsequent works on the EO response of BTO bulk and films revealed a linear change of the refractive index at visible or near-infrared wavelength (400 nm - 1550 nm) with an applied low-frequency electric field, that is a *linear* EO (also called Pockels) [2–7]. In contrast, recent measurements indicate that the EO response of BTO is rather *quadratic* (also called Kerr effect) when measuring the refractive index at 1 THz [8]. To the best of our knowledge, no theoretical work has revealed the origin of this crossover from linear to quadratic in the EO response of barium titanate. Atomistic simulation tools are thus needed to understand the difference between these observations.

Density Functional Theory (DFT) based tools were developed to quantify the linear EO response [9, 10] via the linear EO tensor r_{ij} (using Voigt notation on the first index). Subsequently, the quadratic EO response [11, 12] and its associated tensor R_{ijk} were also determined *ab-initio*. DFT revealed microscopic insights and engineering strategies such as applying bi-axial strain [13], controlling the electrical polarization [14] or nanoscale layering [15] to improve the EO response. However, these methods are limited to 0 K and fail in describing the EO response of BTO in its room temperature, tetragonal phase [16, 17] because of the soft phonon modes with imaginary frequency calculated in this phase [9]. Very recently, Kim *et al.* worked around that problem by treating the tetragonal phase of BTO as the average of four monoclinic structures [19]. Yet, that approach remains limited to the linear EO response, and cannot explain the emergence of the quadratic EO response at 1 THz. Alternatively, Veithen *et al.* [28] mapped the dependency of the electronic dielectric constant with respect to the amplitude of the soft ferroelectric mode and strain from DFT calculations at 0 K. Subsequently, they used an effective Hamiltonian and Monte Carlo simulations, a process that has successfully described the finite temperature properties of ferroelectrics over the years [20–27], to derive the linear EO constants in the thermal stability window of the tetragonal phase of BTO. However, the pioneering approach developed by Veithen *et al.* did not derive the quadratic EO constant, which is necessary to explain the transition from linear to quadratic EO regime in BTO. Moreover, this approach is neither

applicable to THz frequencies nor allows the computations of EO responses in more complex and promising systems, such as (Ba,Sr)TiO_3 (BST) disordered solid solutions.

Here, we derive the methodology to compute the non-linear or Kerr EO response of ferroelectrics at finite temperature. We also highlight a missing term in the linear EO response derived in Ref. [28], which is important to the EO response for THz electromagnetic waves. We then implement these derivations within the effective Hamiltonian scheme and reveal why the EO response in BTO is mostly linear when visible light is employed, *versus* mostly quadratic when using THz radiation. We finally describe how BST solid solutions may enhance the EO response.

Let us first start with the expression of the unclamped linear EO coefficients [31]:

$$r^{\sigma}_{ij\gamma}(\omega,\nu) = \left(\frac{\partial}{\partial E_\gamma(\nu)}\right)_\sigma \left(\frac{1}{\varepsilon^\sigma(\omega)}\right)_{ij} \tag{1}$$

with ω the angular frequency of the light, ν the frequency of the applied electric field E. i, j and γ are cartesian indices; E_γ is the γ component of the applied electric field. $\left(\frac{1}{\varepsilon^\sigma(\omega)}\right)_{ij}$ is the tensor of the inverse dielectric permittivity at frequency ω. The label σ indicates that we consider the unclamped EO coefficients, *i.e.*, in constant stress conditions.

These linear coefficients can be rewritten in the following way (cf. Ref. [28]):

$$r^{\sigma}_{ij\gamma}(\omega,\nu) = r^{\sigma,el}_{ij\gamma}(\omega,\nu) + r^{\sigma,ion}_{ij\gamma}(\omega,\nu) + r^{\sigma,el-ion,pol}_{ij\gamma}(\omega,\nu) + r^{\sigma,el-ion,strain}_{ij\gamma}(\omega,\nu)$$

with :

$$\begin{aligned}
r^{\sigma,el}_{ij\gamma}(\omega,\nu) &= -\frac{1}{n_i^2(\omega)n_j^2(\omega)}\chi^{(2)el,\sigma}_{\gamma ij}(\omega,\nu)\\
r^{\sigma,ion}_{ij\gamma}(\omega,\nu) &= -\frac{1}{n_i^2(\omega)n_j^2(\omega)}\chi^{(2)sm,\sigma}_{\gamma ij}(\omega,\nu)\\
r^{\sigma,el-ion,pol}_{ij\gamma}(\omega,\nu) &= -\frac{1}{n_i^2(\omega)n_j^2(\omega)}\varepsilon_0\sum_\alpha\left(\frac{\partial}{\partial P_\alpha}\varepsilon^{el,\sigma}_{ij}(\omega)\right)_{\boldsymbol{\eta}}\chi^{sm,\sigma}_{\alpha\gamma}(\nu)\\
r^{\sigma,el-ion,strain}_{ij\gamma}(\omega,\nu) &= -\frac{1}{n_i^2(\omega)n_j^2(\omega)}\sum_{\mu,\beta}\left(\frac{\partial}{\partial \eta_{\mu\beta}}\varepsilon^{el,\sigma}_{ij}(\omega)\right)_{\mathbf{P}} d^{\sigma}_{\gamma\mu\beta}(\nu)\\
n_i(\omega) &= \sqrt{\varepsilon^{el,\sigma}_{ii}(\omega) + \chi^{sm,\sigma}_{ii}(\omega)}
\end{aligned} \tag{2}$$

where all derivatives are partial, at either constant strain η or constant polarization $\mathbf{P}$. $\varepsilon^{el,\sigma}_{ij}$ is the electronic dielectric permittivity, and $\chi^{(2)el,\sigma}_{\gamma ij}$ is the nonlinear electronic dielectric susceptibility [28]. $\chi^{sm,\sigma}_{\alpha\gamma} = \frac{dP_\alpha}{\varepsilon_0 dE_\gamma}$ is the dielectric susceptibility associated with the soft mode (the soft mode is proportional to the polarization). $\chi^{(2)sm,\sigma}_{\gamma ij}(\omega,\nu)$ is the nonlinear susceptibility related to that soft mode (*i.e.*, which corresponds to the first derivatives with respect

to the electric field of the soft-mode related susceptibility). $d^{\sigma}_{\gamma\mu\beta} = \frac{d\eta_{\mu\beta}}{dE_{\gamma}}$ are piezoelectric coefficients. The third term in Eq. (2) describes how, under an applied electric field, the soft-mode amplitude is modified and alters the refractive indices. Similarly, the last term on the right hand side of Eq. (2) translates how piezoelectric effects change the unit cell shape and result in a modification of the dielectric response at frequency $\omega/2\pi$.

Equation (2) is similar to Equation (2) in Ref. [28], except for the presence, here, of the second term, $r^{\sigma,ion}_{ij\gamma}(\omega,\nu)$. This is one of the (important) novelties of the present work, which were not considered in past works [28–30]. It is related to the nonlinear dielectric susceptibility associated with the soft mode and is important for some frequencies such as THz. One has also to realize that the second and third terms of Eq.(2) generally should involve a sum over all infra-red (IR) and Raman-active optical phonons [28]. Yet, we show below that only incorporating the soft-mode already captures most of the EO effect in BTO and BST. Indeed, the other IR and Raman-active phonons contribute little in the specific case of BTO, owing to their relative small polarizability and Raman susceptibility compared to the soft mode [9].

Technically, Eq. (2) assumes that $\nu \ll \omega$, in order that the applied electric field frequency ν does not appreciably change the frequency $\omega/2\pi$ of the electromagnetic radiation [4]. In our subsequent calculations, we employ $\nu = 0$ – that is we focus on *static* applied electric fields.

Let us also derive an analytical expression for the (unclamped) quadratic EO coefficients, in order to be able to compute them in the same conditions as the linear ones. For that, we assume that the main dependence on the electric field in Eq. (2) arises from the soft-mode related dielectric susceptibilities. Such assumption is valid close to structural phase transitions or when ω ranges in the THz regime (which are typical vibration frequencies of electrical polarization). Within this assumption, the nonlinear quadratic EO coefficients can therefore be obtained by taking the full derivative of the soft-mode susceptibilities with respect to the electric field in Equation (2). For example, $\chi^{(2)sm,\sigma}_{\beta ij}(\omega)$ in Eq. (2) becomes $\chi^{(3)sm,\sigma}_{\alpha\beta ij} = \frac{d\chi^{sm,\sigma}_{ij}}{dE_{\alpha}dE_{\beta}}$ and so on. One thus arrives at:

$$R_{ij\alpha\beta}(\omega,\nu,\nu) \approx R^{ion}_{ij\alpha\beta}(\omega,\nu,\nu) + R^{el-ion,pol}_{ij\alpha\beta}(\omega,\nu,\nu)$$

with :

$$\begin{aligned} R^{ion}_{ij\alpha\beta}(\omega,\nu,\nu) &= -\tfrac{1}{n_i^2(\omega)n_j^2(\omega)}\chi^{(3)sm,\sigma}_{\alpha\beta ij}(\omega,\nu,\nu) \\ R^{el-ion,pol}_{ij\alpha\beta}(\omega,\nu,\nu) &= -\tfrac{1}{n_i^2(\omega)n_j^2(\omega)}\varepsilon_0 \textstyle\sum_\gamma \left(\frac{\partial}{\partial P_\gamma}\varepsilon^{el,\sigma}_{ij}(\omega)\right)_{\boldsymbol{\eta}} \chi^{(2)sm,\sigma,}_{\beta\alpha\gamma}(\nu,\nu) \\ n_i(\omega) &= \sqrt{\varepsilon^{el,\sigma}_{ii}(\omega) + \chi^{sm,\sigma}_{ii}(\omega)} \end{aligned} \tag{3}$$

Theoretically, the first and second terms in Eq. (3) should also involve a sum over all IR-active and Raman-active phonon modes. However, considering only the soft mode seems enough to capture the quadratic EO coefficients of BTO films in the THz range as shown below.

We now implement these equations to obtain the finite temperature EO properties in a $Ba_{1-x}Sr_xTiO_3$ (BST) solid solution system, of which BTO bulk is a special case ($x = 0$). We first perform calculations of the electronic dielectric constant in the tetragonal phase of BST for different values of the soft mode amplitude and strain, using the Abinit code [32] with optimized norm-conserving Vanderbilt pseudopotentials ONCVPSP-3.2.3 [33] and the virtual crystal alloy approximation [34], for which Ba and Sr ions are replaced by a composition - dependent virtual ion [35]. We compute here the electronic dielectric constant at $\hbar\omega = 1.55$ eV (corresponding to a wavelength of 800 nm) and at $\hbar\omega = 4$ meV (corresponding to 1 THz radiation) at different displacements of the soft mode and different strains (see Supplementary Materials). We use these values to calculate the derivatives of $\varepsilon^{el,\sigma}_{ij}(\omega)$ with respect to the soft mode and strains using finite differences. $\chi^{(2)el,\sigma}_{\gamma ij}$, in the first term of Equation (2), is calculated directly *ab initio* from the Abinit code at $\hbar\omega = 1.55$ eV and 4 meV as well. Then, we use an effective Hamiltonian describing the energetic couplings between the soft mode and strains for the BST system [23, 25, 36], and perform Monte Carlo Metropolis and Molecular Dynamics simulations *at room temperature* to obtain the soft-mode related linear and non-linear susceptibilities involved in Eqs. (2-3), as well as the piezoelectric constants. More technical details are presented in the Supplementary Information. All these quantities now allow us to calculate the finite temperature linear and quadratic EO response of BST.

Let us first focus on BTO bulk. Comparison with experimental values [4] or previous

calculations show the same qualitative trends: an extremely large value of the r^{σ}_{51} coefficient (≈ 502 pm/V versus $1,300$ pm/V [4]), followed by a significant r^{σ}_{33} (≈ 73.9 pm/V here versus 108 pm/V [4]) and a smaller r^{σ}_{13} (≈ 27 pm/V here versus 8 pm/V [4]). Quantitative differences can be attributed to (1) differences in numerical parametrization or sample quality, leading to different critical temperatures and (2) in our case and in Ref. [28], the neglect of higher frequency IR or Raman-active modes. Yet, incorporating only the soft mode already gives a realistic representation of the EO response of BTO. Among all contributions involved in Eq. (2), $r^{\sigma,el-ion,pol}_{ij\gamma}(\omega,0)$ accounts for most of the reported value (95% of r^{σ}_{33}, 125% of r^{σ}_{13} and 103% of r^{σ}_{51}). It is then clear that the comparatively large value of r^{σ}_{51} compared to r^{σ}_{33} and r^{σ}_{13} originates from the larger dielectric susceptibility $\chi^{sm,\sigma}_{11}$ as we approach the tetragonal-to-orthorombic phase transition in BTO, governed by the softening of the E-modes. In contrast, $\chi^{sm,\sigma}_{33}$ is smaller, as it is mainly contributed to by the A-mode which does not soften during the tetragonal-to-orthorombic phase transition occurring slightly below room temperature.

We now calculate the linear EO constant, but for a THz electromagnetic radiation ($\hbar\omega =$ 4 meV), in bulk BTO. Note that we expect bulk BTO to behave similarly to the BTO thick films deposited on $SrTiO_3$ (STO) measured in Ref. [8]. Indeed, the large thickness of the film, as well as the agreement between their measured lattice constants and our DFT calculated ones (see Supplementary Information) indicate that the strain in BTO thick film is relaxed and that it can be reasonably modeled using bulk BTO. Figure (1a) shows the longitudinal Pockels constant r^{σ}_{33} for both $\hbar\omega = 4$ meV and 1.55 eV, as well as their decomposition on the various terms detailed in Equation (2). The THz linear EO response (≈ 153.2 pm/V) is more than twice as strong as the visible EO constant. Quite interestingly, while the visible EO constant primarily originates from the third term in Equation (2), $r^{\sigma,el-ion,pol}_{33}$, the linear EO response in the THz regime mainly comes from the intrinsic second-order soft-mode related susceptibility $r^{\sigma,ion}_{33}$ (second term in Equation (2)). In other words, this overlooked term in past studies [28–30] is very significant for incident THz electromagnetic radiation indeed.

We now calculate the non-linear EO coefficient R_{333} following Equation (3) in BTO at 300 K, for both visible ($\hbar\omega = 1.55$ eV) and THz ($\hbar\omega = 4$ meV) radiations. Table I shows that the quadratic EO coefficient is enhanced by a factor of 20 in the THz region of the electromagnetic spectrum with respect to visible light. Strikingly, our predicted

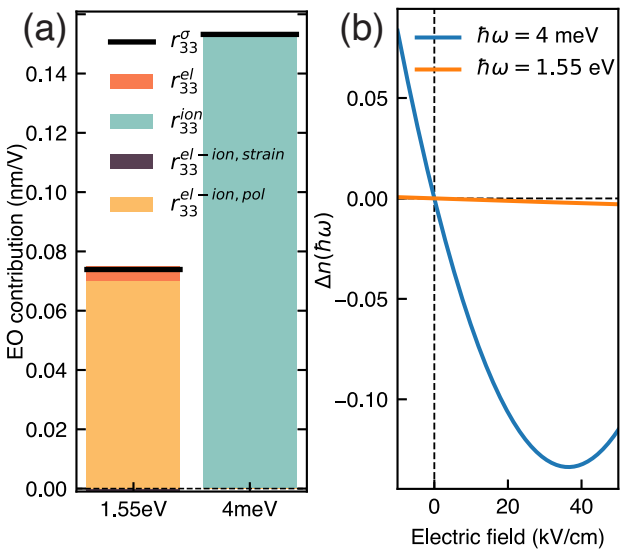

FIG. 1. (a) contributions to the linear EO constant r_{33}^{σ} in BTO at $\hbar\omega = 4$ meV and 1.55 eV. (b) The change of the refractive index Δn for BTO at $\hbar\omega = 4$ meV (in blue) and $\hbar\omega = 1.55$ eV (in orange)

quadratic EO coefficient at 1 THz, $R_{333} = -2.1 \times 10^{-17}\ m^2/V^2$, has the same order of magnitude than experimentally reported ($-1.4 \times 10^{-17}\ m^2/V^2$ in Ref. [8]), which confirms the accuracy and assumptions of the present method. The main contributor to R_{333} in the BTO system comes from the first term in Eq. (3), $R_{333}^{ion}(\omega, \nu = 0, \nu = 0)$, containing the third harmonic of the soft-mode susceptibility. We can thus also explain the discrepancy between the previously DFT calculated value of $6.4{\times}10^{-20}$ m^2/V^2 [11] and the 200 times larger experimental value reported by Chen et al. [8]. Indeed, the DFT scheme developed in Ref. [11] does not account for this third harmonic soft-mode related susceptibility. To explore the linear *versus* quadratic nature of the EO induced change in refractive index in BTO, we calculate the change of optical index $\Delta n(\hbar\omega)$ using the formula [39]:

$$\Delta n = -\tfrac{1}{2}\left(\varepsilon_{33}^{tot,\sigma}\right)^{3/2} \mathcal{R}_{33} \tag{4}$$

$$with$$

$$\varepsilon_{33}^{tot,\sigma} = \varepsilon_{33}^{el,\sigma}(\hbar\omega) + \chi_{33}^{sm,\sigma}(\hbar\omega)$$

$$\mathcal{R}_{33} = \left[r_{33}(\hbar\omega, \nu = 0) + R_{333}(\hbar\omega, \nu = 0, \nu = 0) E_3(\nu = 0)\right] E_3(\nu = 0)$$

We plot the estimated change of the optical indices for reasonable values of the electric field applied along the polar axis of BTO in Figure (1b). Interestingly, the orange curve,

$\hbar\omega$	r_{33}^{σ} (pm/V)	R_{333} (m^2/V^2)	$\varepsilon_{33}^{el,\sigma}(\omega)$	$\chi_{33}^{sm,\sigma}(\omega)$
1.55 eV	73.9	-1.1×10^{-18}	6.8	0
4 meV	153	-2.1×10^{-17}	6.3	91

TABLE I. Summary of the linear and quadratic EO constants, electronic dielectric constant and soft-mode related dielectric susceptibility in BTO bulk for visible light ($\hbar\omega = 1.55$ eV) or THz ($\hbar\omega = 4$ meV) incoming radiation, at 300 K.

corresponding to visible light ($\hbar\omega = 1.55$ eV), shows a linear EO response with small magnitude. In contrast, the THz EO response (in blue in Figure (1b)) is clearly quadratic and is strongly enhanced compared to the visible EO response. The much larger change in THz optical index seen in Figure (1b) can be attributed to (i) the larger quadratic EO constant R_{333} stemming from the third harmonic of the soft-mode susceptibility and (ii) the large increase in the THz dielectric constant $\varepsilon_{33}^{tot,\sigma} = \varepsilon_{33}^{el,\sigma} + \chi_{33}^{sm,\sigma}$ (see Table I and Equation 4). Dispersions of the EO coefficients and dielectric response in BTO (see Supplementary Material) indicate that the crossover from linear to quadratic EO response occurs through a transition region dominated by optical phonon dielectric resonances. This transition region extends from the lowest IR- and Raman-active optical phonon frequency (in our case, about 38 meV) to the frequency at which the electronic dielectric response supersedes the ionic one. Similar crossover for in-plane applied electric fields are expected due to the close frequency (41 meV) of the soft ferroelectric E mode.

Now that the apparent discrepancy between various measurements in BTO films is resolved, we shift our focus to BST with varying compositions x and visible wavelength (800 nm, or $\hbar\omega = 1.55$ eV). We evidence there that, as x increases, we gradually change from a mostly linear EO response to a non-linear, quadratic EO change of optical index. It is well-known that, as x increases, the tetragonal-to-cubic transition temperature decreases in BST, reaching 300 K around $x = 26$ %. [23] One would then expect that the soft-mode susceptibility $\chi_{33}^{sm,\sigma}$ diverges, resulting in large r_{33}^{σ} and r_{13}^{σ} around this particular concentration. This is indeed what is observed in Figure (2a), causing r_{33}^{σ} to exceed r_{51}^{σ}. We also calculated the quadratic EO coefficient R_{333} following Eq. (3). Interestingly, R_{333} also increases strongly for compositions near the tetragonal-to-cubic transition at 300 K (see Figure 2b) due to softening of the E-modes towards this border, which leads to divergence of

the third-order susceptibility $\chi^{(3)sm,\sigma}_{\alpha\beta ij}(\omega,0,0)$ in the first term of Equation 3, $R^{ion}_{ij\alpha\beta}(\omega,0,0)$. One could therefore reasonably expect a strong enhancement of the optical index change $\Delta n(\hbar\omega)$ near $x = 26$ % when applying an electric field E_3 along the [001] direction. We, in fact, calculated the expected change in optical index at $\hbar\omega = 1.55$ eV using Equation (4) and report it in Figure (2c).

We find, at low x, that the change in optical index is mostly linear; however, for x approaching 26 %, Δn now adopts a strong non-linear (quadratic) dependency on the applied static electric field at($\hbar\omega = 1.55$ eV. Figure (2c) also stresses the importance of carefully choosing the direction and sign of the applied electric field to maximize the EO change of optical index. Indeed, the large quadratic response occurring at the phase transition competes with the linear EO response for positive biases applied in the direction of the polarization, severely limiting the change of optical index. This outlines the need to not only consider the linear EO response at phase transitions, as done in previous works [13], but consider higher orders such as the quadratic EO response as well. The methods developed in this work present one of the very few attempts to comprehensively include higher order effects in the EO characterization of ferroelectrics. One may define a crossover electric field in Figure (2d) as $-\frac{r^{\sigma}_{33}}{R_{333}}$. It corresponds to the electric field above which the quadratic EO response supersedes the linear one. Figure (2d) shows that this crossover field continuously decreases as x increases, and vanishes at the tetragonal-to-cubic transition.

In summary, the coupled DFT-effective Hamiltonian scheme presented here is able to calculate linear and quadratic EO responses at finite temperature, for various frequencies and in simple BTO but also BST solid solutions. It is also revealed that a previously overlooked term involving the non-linear dielectric susceptibility related to the soft ferroelectric mode is instrumental to correctly understand the EO response of classical ferroelectrics in the THz regime. Thanks to these tools, we have explained the crossover from the linear to quadratic EO response in barium titanate when using visible or THz electromagnetic radiation. Furthermore, our general effective Hamiltonian scheme also reveals that (and explain why) the quadratic EO response may be significantly enhanced as well in the vicinity of structural phase transitions such as the composition-driven tetragonal-to-cubic phase transition in BST. The universality of this coupled DFT-effective Hamiltonian scheme should allow to explore the finite temperature response of more complex polar systems, for instance exhibiting second order [21, 40] or order-disorder ferroelectric phase transitions [41–43].

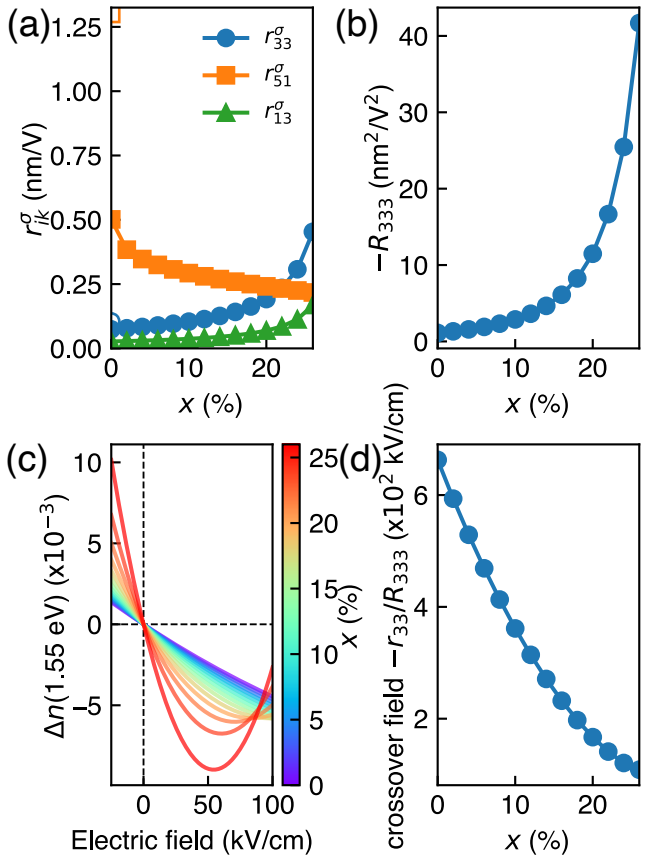

FIG. 2. (a) Calculated linear EO constants versus composition x in bulk BST; open symbols denote experimental values [4]. (b) Computed quadratic EO constant R_{333} *versus* composition x. (c) Expected change of refractive index for electric fields along the polar direction. (d) Crossover field at which the linear and quadratic contributions to the change of refractive index are equal. All data were calculated at 300 K and for $\hbar\omega = 1.55$ eV.

The authors thank the support of Grant number FA9550-23-1-0500 from ONR (Depscor) and of Grant number PA-23-01-03-ATOM-FP-004 from DARPA.

* sprossan@uark.edu

† paillard@uark.edu

‡ laurent@uark.edu

[1] K. Buse, A. Adibi, and D. Psalti, *Nature* (London) **393**, 665 (1998).

[2] A. R. Johnston and J. M. Weingart, *J. Opt. Soc. Am.* **55**, 828 (1965).

[3] A. R. Johnston, *Appl. Phys. Lett.* **7**, 195 (1965).

[4] M. Zgonik *et al.*, *Phys. Rev. B* **50**, 5941 (1994).

[5] P. Bernasconi, M. Zgonik, and P. Günter, *J. Appl. Phys.* **78**, 2651 (1995).

[6] S. Wang *et al.*, *Adv. Mater.* **34**, 2207261 (2022).

[7] Y. Cao *et al.*, *Opt. Mater. Express* **13**, 152 (2023).

[8] L. Chen *et al.*, *Appl. Phys. Lett.* **105**, 112903 (2014).

[9] M. Veithen, X. Gonze, and P. Ghosez, *Phys. Rev. Lett.* **93**, 187401 (2004).

[10] M. Veithen, X. Gonze, and P. Ghosez, *Phys. Rev. B* **71**, 125107 (2005).

[11] Z. Jiang *et al.*, *Phys. Rev. Lett.* **125**, 017401 (2020).

[12] Z. Jiang *et al.*, *Phys. Rev. B* **106**, L081404 (2022).

[13] C. Paillard, S. Prokhorenko, and L. Bellaiche, *npj Comput. Mater.* **5**, 6 (2019).

[14] F. Delodovici *et al.*, *J. Appl. Phys.* **134**, 055108 (2023).

[15] Z. Jiang *et al.*, *Phys. Rev. Lett.* **123**, 096801 (2019).

[16] H. D. Megaw, *Acta Crystallogr.* **5**, 739 (1952).

[17] G. H. Kwei *et al.*, *J. Phys. Chem.* **97**, 2368 (1993).

[18] Ph. Ghosez *et al.*, *Phys. Rev. B* **60**, 836 (1999).

[19] I. Kim, T. Paoletta, and A. A. Demkov, *Phys. Rev. B* **108**, 115201 (2023).

[20] W. Zhong, D. Vanderbilt, and K. M. Rabe, Phys, Rev. B **52**, 6301 (1995).

[21] L. Bellaiche, A. GarcÃa, and D. Vanderbilt, *Phys. Rev. Lett.* **84**, 5427 (2000).

[22] I. A. Kornev *et al.*, *Phys. Rev. Lett.* **97**, 157601 (2006).

[23] L. Walizer, S. Lisenkov, and L. Bellaiche, *Phys. Rev. B* **73**, 144105 (2006).

[24] I. A. Kornev *et al.*, *Phys. Rev. Lett.* **99**, 227602 (2007).

[25] S. Lisenkov and L. Bellaiche, *Phys. Rev. B* **76**, 020102 (2007).

[26] I. C. Infante *et al.*, *Phys. Rev. Lett.* **105**, 057601 (2010).

[27] D. Sando *et al.*, *Nat. Mater.* **12**, 641 (2013).

[28] M. Veithen and Ph. Ghosez, *Phys. Rev. B* **71**, 132101 (2005).

[29] S. Kondo, T. Yamada, A. Tagantsev, N. Setter, M. Yoshino and T. Nagasaki, *J. Ceram. Soc. Jap.* **127**, 348 (2019).

[30] Y. Liu, G. Ren, T. Cao, R. Mishra, J. Ravichandran, *J. Appl. Phys.* **131**, 163101 (2022).

[31] F. Pockels, Goettinger Abhandl (in German), 39 (1894); F. Pockels, Lehrbuch der Kristalloptik (in German), Leipzig (1906).

[32] X. Gonze, J.-M. Beuken, R. Caracas, F. Detraux, M. Fuchs, G.-M. Rignanese, L. Sindic, M. Verstraete, G. Zerah, F. Jollet, M. Torrent, A. Roy, M. Mikami, P. Ghosez, J.-Y. Raty, and D. C. Allan, Comput. Mater. Sci. **25**, 478 (2002).

[33] D. R. Hamann, Phys. Rev. B **88**, 085117 (2013).

[34] L. Bellaiche and D. Vanderbilt, *Phys. Rev. B* **61**, 7877 (2000).

[35] A. Castellano, F. Bottin, B. Dorado, and J. Bouchet, Phys. Rev. B textbf101, 184111 (2020).

[36] R. Walter *et al.*, *npj Comput. Mater.* **6**, 186 (2020).

[37] N. A. Pertsev, A. G. Zembilgotov, and A. K. Tagantsev, *Phys. Rev. Lett.* **80**, 1988 (1998).

[38] N. A. Pertsev, A. G. Zembilgotov, and A. K. Tagantsev, Ferroelectrics **223**, 79 (1999).

[39] D. Sando *et al.*, *Appl. Phys. Rev.* **5**, 041108 (2018).

[40] L. Bellaiche, A. Garcia and D. Vanderbilt, *Ferroelectrics* **266**, 41 (2002).

[41] R. Pirc and R. Blinc, *Phys. Rev. B* **70**, 134107 (2004).

[42] J. Hlinka, T. Ostapchuk, D. Nuzhnyj, J. Petzelt, P. Kuzel, C. Kadlec, P. Vanek, I. Ponomareva and L. Bellaiche, *Phys. Rev. Lett.* **101**, 167402 (2008).

[43] I. Ponomareva, L. Bellaiche, T. Ostapchuk, J. Hlinka and J. Petzelt, *Physical Review B* **77**, 012102 (2008).